PHYSICS

Solid-state spin coherence time approaching the physical limit

Shuo Han[1,2]†, Xiangyu Ye[1,2]†, Xu Zhou[1,2,3]†, Zhaoxin Liu[1,2], Yuhang Guo[1,2], Mengqi Wang[1,2], Wentao Ji[1,2], Ya Wang[1,2,3]*, Jiangfeng Du[1,2,3,4]

Extending the coherence time of quantum systems to their physical limit is a long-standing pursuit and critical for developing quantum science and technology. By characterizing all the microscopic noise sources of the electronic spin [nitrogen-vacancy (NV) center] in diamonds using complete noise spectroscopy, we observe a previously unforeseen noise spectrum manifested as the empirical limit ($T_2 \approx \frac{1}{2}T_1$) that has puzzled researchers for decades in various solid-state systems. By implementing a corresponding dynamical decoupling strategy, we are able to surpass the empirical limit and approach the upper physical limit $T_2 = 2T_1$ for NVs, from room temperature down to 220 kelvin. Our observations, including the independence across different spatial sites and its dependence on temperature in the same way as spin-lattice relaxation, suggest an emerging decoherence mechanism dominated by spin-lattice interaction. These results provide a unified and universal strategy for characterizing and controlling microscopic noises, thereby paving the way for achieving the physical limit in various solid-state systems.

INTRODUCTION

Exploring the physical limits of physical systems represents a critical frontier with far-reaching implications for both fundamental research and technological development. In modern science, quantum technologies promise to surpass classical counterparts by leveraging quantum coherence. However, quantum systems inevitably encounter challenges in maintaining their quantum coherence due to various noises and dissipation. For all qubits, the dissipation with a characteristic relaxation time T_1 imposes an upper limit on the coherence time T_2, known as $T_2 = 2T_1$ (*1*). Reaching this limit would have profound implications for realizing the quantum revolution, including largely reducing the overhead in quantum computing (*2*, *3*), achieving optimal quantum sensing (*4*, *5*), and establishing large-scale quantum networks (*6*, *7*).

However, achieving this goal is challenging, especially for solid-state spin systems, which have emerged as promising candidates for scalable quantum networks and nanoscale quantum sensing (*8*–*19*). Substantial efforts have been devoted to both active isotopically engineered processes (*20*, *21*) and passive dynamical decoupling (DD) techniques (*22*–*30*). Despite notable progress achieved in recent decades, the spin coherence time of all these solid-state spin systems remains intriguingly restricted to an empirical limit $T_2 \approx \frac{1}{2}T_1$ (Fig. 1A), which dates back to the historical study of electron paramagnetic resonance (*31*). This broad and long-standing puzzle suggests the existence of undiscovered physical mechanisms beyond the previous scope of material engineering and DD techniques. Therefore, addressing this intricate physical mechanism represents a key step toward advancing quantum technology.

In this paper, we quantitatively identify the underlying microscopic interaction mechanisms within diamond material using a unified and universal approach developed here. We show that this mechanism exhibits a unique nonlocal nature distinct from the conventional spin-lattice relaxation. By decoupling this interaction, we enable the nitrogen-vacancy (NV) center to surpass the empirical limit and achieve the longest room-temperature coherence time of 4.34 ms ever observed for solid-state electronic spins (*20*, *21*, *24*, *29*).

RESULTS

The discrepancy between empirical limit and physical limit for NV centers

Our experiments use individual NV centers ($S = 1$) in diamond crystals for illustration. To verify the limit discrepancy, we measured a spin qubit composed of the $m_s = 0$ and $m_s = -1$ states from the spin-triplet (Fig. 1B) under a magnetic field around 400 G. A standard Carr-Purcell-Meiboom-Gill (CPMG) sequence (Fig. 1D, top) was applied to obtain the coherence time T_2 by extracting $T_{2,\mathrm{CPMG}}$ as the pulse number increased (Fig. 1D, middle), until it reached saturation (Fig. 1D, bottom). For the T_1 measurement, two additional dissipation channels from the qubit subspace to the $m_s = +1$ state need to be considered. These channels are characterized by $\Omega_\perp(\omega_{0,+1})$, representing the transition rate between $m_s = 0$ and $m_s = +1$, and $\gamma_\perp(\omega_{-1,+1})$, representing the transition rate between $m_s = -1$ and $m_s = +1$ (Fig. 1B). Together with the transition rate $\Omega_\perp(\omega_{0,-1})$, these rates determine the relaxation time T_1 (see section S1.A). To extract the specific transition rate, two groups of sequences were applied (Fig. 1C, top) with the results shown in Fig. 1C (bottom). Last, the results of three randomly selected NV centers, as displayed in Fig. 1E, show that T_2 is still restricted by the empirical limit for $S = 1$ spin systems (as detailed in Materials and Methods) and remains far from the physical limit.

This discrepancy suggests the presence of an undiscovered noise mechanism. To investigate this, we analyze both the CPMG and spin-relaxation measurements in terms of noise spectroscopy. As illustrated in Fig. 2, we resolve the axial noise spectrum density

[1]CAS Key Laboratory of Microscale Magnetic Resonance and School of Physical Sciences, University of Science and Technology of China, Hefei 230026, China. [2]Anhui Province Key Laboratory of Scientific Instrument Development and Application, University of Science and Technology of China, Hefei 230026, China. [3]Hefei National Laboratory, University of Science and Technology of China, Hefei 230088, China. [4]Institute of Quantum Sensing and School of Physics, Zhejiang University, Hangzhou 310027, China.
*Corresponding author. Email: ywustc@ustc.edu.cn
†These authors contributed equally to this work.

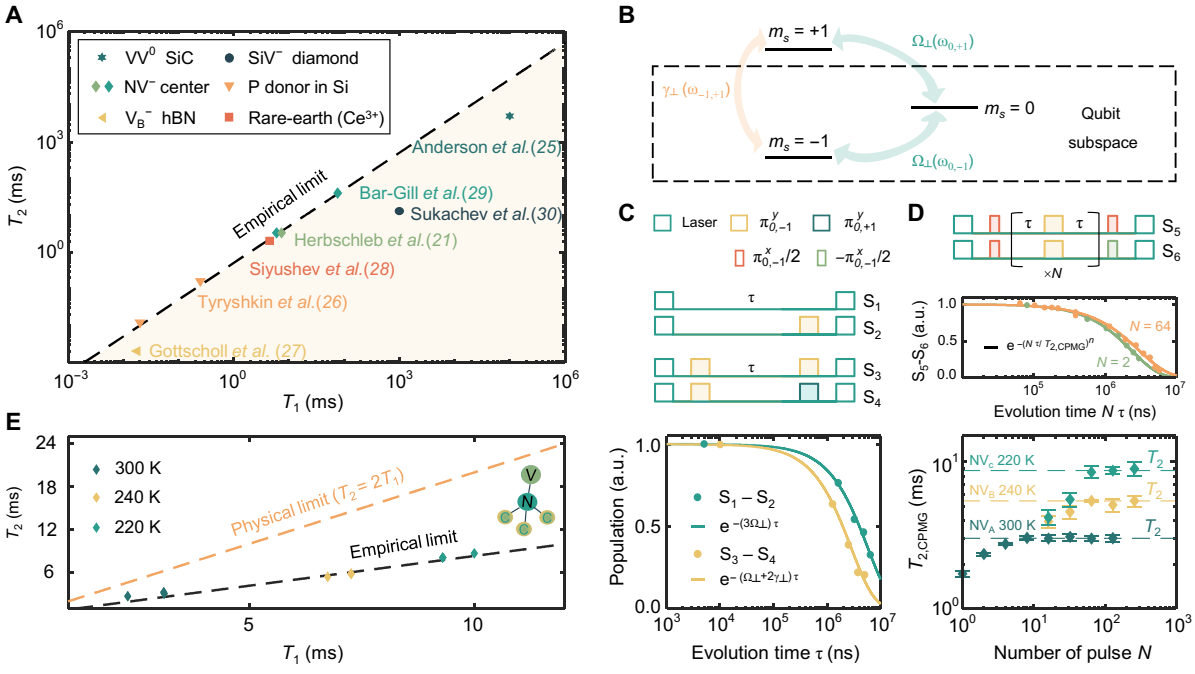

Fig. 1. Solid-state spin coherence time limit. (**A**) The reported coherence time (T_2) of solid-state spins, including $S = 1$ systems such as VV^0 in SiC (*25*), NV center in diamond (*21*, *29*), and V_B^- in hBN (*27*), as well as $S = 1/2$ systems like P donor in silicon (*26*), single-electron spin of rare-earth ion (Ce^{3+}) (*28*), and SiV^- in diamond (*30*), follows the empirical limit. (**B**) The level structure of the NV's electronic spin ($S = 1$) and the dissipation channels between these levels are shown. Under a magnetic field around 400 G, the energy difference $\omega_{0,-}$, $\omega_{0,+}$, and $\omega_{-1,+1}$ are all around gigahertz. In the qubit's subspace, its relaxation time could be simplified as $T_1 = 1/(3\Omega_\perp + \gamma_\perp)$, assuming $\Omega_\perp(\omega_{0,+1}) = \Omega_\perp(\omega_{0,-1}) = \Omega_\perp$ and $\gamma_\perp = \gamma_\perp(\omega_{-1,+1})$. (**C**) The measurement sequence for $\Omega_\perp$ and $\gamma_\perp$, where $\Omega_\perp$ is extracted from $S_1 - S_2$, and $\gamma_\perp$ is extracted from $S_3 - S_4$. a.u., arbitrary units. (**D**) The CPMG sequence for measuring $T_{2,CPMG}$ and the process to extract $T_{2,CPMG}$ at different pulse numbers. T_2 is determined once $T_{2,CPMG}$ approaches a steady value as the pulse number (N) increases. (**E**) The measured T_2 and T_1 follow the empirical limit for NV centers at different sites and different temperatures.

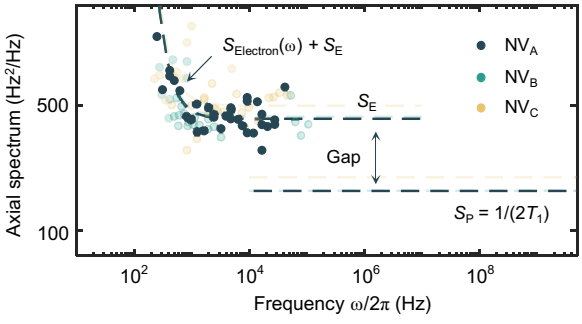

Fig. 2. Axial noise spectrum density exhibiting a gap between empirical and physical limits. Reconstructed axial noise spectrum density derived from the CPMG data for NV_A, NV_B, and NV_C at 300 K, where the impurity electron spin noise [$S_{Electron}(\omega)$; fig. S4] dominates the part with $\omega/2\pi < 1$ kHz.

(*32*, *33*) from the CPMG data in Fig. 1D (see section S3.A). The CPMG results yield a Lorentzian spectrum in the low-frequency regime ($\omega/2\pi < 1$ kHz), with a baseline intensity (S_E) responsible for the observed empirical limit ($\omega/2\pi > 1$ kHz). In contrast, the noise intensity (S_P) from the spin-relaxation results determines the coherence physical limit. As expected, the noticeable disparity between these two limits suggests the existence of an emerging noise mechanism within the frequency range (from kilohertz to gigahertz).

Therefore, to surpass the long-standing empirical limit, it is crucial to characterize the profile of the missing noise spectrum in such a broad frequency range and develop a corresponding noise-suppression strategy.

Relaxation noise spectroscopy characterizing the spectrum profile

To cover a broad frequency range, we leverage the capability of spin-relaxation measurements to tune the spin energy across a wide dynamic range by simply varying the magnetic field (Fig. 3A). However, this spectroscopy becomes complicated when the transition frequency approaches the magnitude of other weak hyperfine interactions. For NV centers in diamonds, the hyperfine interaction with the nitrogen nuclear spin ($I = 1$) (*34*) causes the electron spin state strongly mix with nitrogen spin states ($m_I = +1, 0, -1$) as the energy crossing point is approached ($\omega_{0,-1} \sim$ MHz), as shown in Fig. 3B. This interaction alters the qubit's susceptibility to the magnetic field and opens additional relaxation pathways that were previously forbidden. As a result, extracting the relaxation rate at frequencies around megahertz becomes complicated. To address this challenge, we adopt a specific transition (Fig. 3B, orange line; see section S2.B) that is nearly isolated from other states and exhibits an almost unchanged susceptibility ($\eta = \frac{\partial\omega}{-\gamma_e \partial B_z} \sim 0.9$) close to that of a free electron spin.

We thus prepare the initial state as $|m_s = -1, m_I = -1\rangle$ and then measure its relaxation (Fig. 3C; also see section S2.C). This process allows us to accurately determine the relaxation rate $\Omega_\perp(\omega_{0,-1})$ when $\omega_{0,-1} \sim$ MHz and to construct the transverse noise spectrum (Fig. 3D; also see section S2.C), which fills in the missing frequency

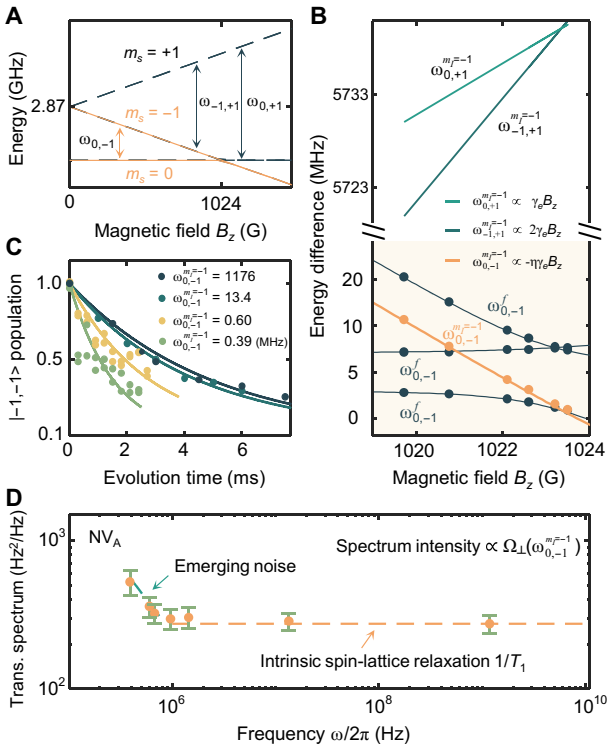

Fig. 3. Relaxation noise spectroscopy revealing an emerging noise mechanism. (**A**) Relaxation spectroscopy relies on the spin state energy difference ($\omega_{0,-}$, $\omega_{0,+}$, or $\omega_{-1,+}$), with the relationship between these differences and the magnetic field shown in (B). (**B**) Near the energy crossing point (1024 G), the relaxation spectroscopy could detect noise intensity at frequencies below a few megahertz ($\omega_{0,-}$) and around 5730 MHz ($\omega_{0,+}$ and $\omega_{-1,+}$). The measured transition frequencies (dots) of $\omega_{0,-1}$ agree well with the theoretical predictions (solid lines). $\omega_{0,-1}^{f}$ denotes transitions that are previously forbidden. A specific transition ($\omega_{0,-1}^{m_I=-1}$) is selected (see section S2.B), with a susceptibility ($\eta \sim 0.9$) close to free electron spin. (**C**) Measured population relaxation, starting from an initial state of $|m_s=-1, m_I=-1\rangle$ to states $|m_s=0, m_I=-1\rangle$ and $|m_s=+1, m_I=-1\rangle$, following the same process as in Fig. 1B. The solid lines are fitting curves (see section S2.C). (**D**) Reconstructed transverse noise spectrum from the varying spin-relaxation rates $\Omega_\perp\left(\omega_{0,-1}^{m_I=-1}\right)$ in (C) (see section S2.C). All error bars are 1σ.

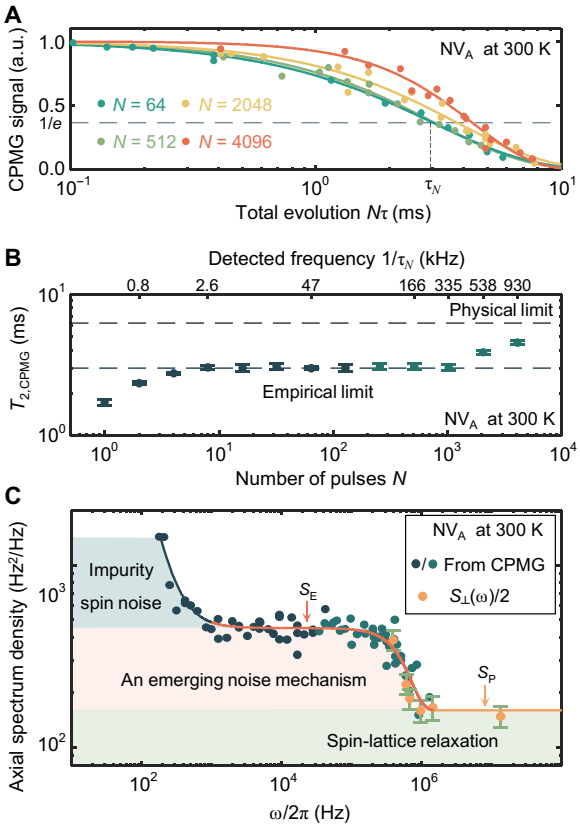

Fig. 4. Approaching the physical limit via complete noise spectroscopy and a corresponding decoupling strategy. (**A**) CPMG results with the number of π pulses up to $N = 4096$. Solid lines are fits to $\sim \exp\left[-\left(N\tau/T_{2,\mathrm{CPMG}}\right)^n\right]$, with $T_{2,\mathrm{CPMG}} = 4.34$ ms for $N = 4096$. The evolution time τ_N denotes the point at which the CPMG-N curve decays to $1/e$. (**B**) Spin coherence time surpasses the empirical limit using CPMG with larger N and smaller τ. The corresponding decoupling frequency is denoted as $1/\tau_N$ in the top axis. (**C**) Complete axial noise spectrum with all the relevant sources clarified in diamonds. The dark solid dots are from Fig. 2, and the green solid dots represent CPMG data from $N = 256$ to $N = 4096$. The orange solid dots are from relaxation measurement data in Fig. 3D. The dashed line is a guideline. All error bars are 1σ.

range in Fig. 2. Notably, in addition to the intrinsic spin relaxation (Fig. 3D, orange line), a distinct noise component (Fig. 3D, green line) emerges at frequencies below 1 MHz, which is inconsistent with conventional electromagnetic noise sources (*35*–*38*). Because the cutoff frequency of this noise lies at the edge of the detection bandwidth of the DD sequence, it suggests that using a CPMG sequence with a decoupling frequency extending into this range could further extend the spin coherence time.

Approaching the physical limit via complete noise spectroscopy

To confirm this prediction, we proceed with CPMG sequences with decoupling frequencies approaching 1 MHz (Fig. 4B, with $N > 128$). As anticipated, a further enhancement of the coherence time, surpassing the empirical limit, is observed once the decoupling frequency exceeds a certain threshold (Fig. 4A). In this process, we achieve a room-temperature coherence time of 4.34 ms, exceeding that observed in previous solid-state electronic spin systems (*20*, *21*, *24*, *29*). Further extension of this $T_{2,\mathrm{CPMG}}$ is limited by the pulse control fidelity, which is halved for $N = 4096$ at room temperature (fig. S8). The reconstructed axial noise spectrum from the CPMG results (Fig. 4C, dark solid dots from $N < 128$ and green solid dots from $N > 128$), aligns well with the transverse noise spectrum (Fig. 4C, orange solid dots).

With all these findings, we thus obtain the complete noise spectrum for NV centers within diamonds (Fig. 4C). This comprehensive spectrum successfully establishes the threshold frequency required for completely decoupling each noise mechanism. Below 1 kHz: The electronic spin bath is the main contributor to the noise spectrum, showing that the interactions between the central spin and its specific surrounding electronic spin bath play a crucial role in spin decoherence. Above 1 MHz: The noise spectrum is dominated by the intrinsic spin relaxation, suggesting that the relaxation of spins to their equilibrium state fundamentally determines the coherence physical limit of a spin qubit within a quantum system. Between 1 kHz and 1 MHz: The spectrum is primarily influenced by a noise source with a high cutoff frequency around 1 MHz. Once the decoupling frequency

exceeds this threshold, we observe that the coherence time surpasses the empirical limit and approaches the physical limit (Fig. 5A, orange pentagram and extracted from the longest coherence time of $T_{2,\mathrm{CPMG}}$). In particular, these similar behaviors observed across different NVs at varying temperatures potentially suggest this emerging noise's nonlocal and temperature-dependent nature.

A spin-lattice interaction dominated by delocalized modes

To further quantify these characteristics, we conduct the experimental characterization and find that the intensity of this emerging noise ($S_E - S_P$) obtained from randomly selected NV center sites demonstrates a site-independent behavior (Fig. 5B). This nonlocal nature stands in stark contrast to the previously observed magnetic noises, electrical noises, or spin-lattice relaxation, which highly depends on the local microscopic environment [local density of spin (*39*, *40*), charge (*11*, *35*, *41*, *42*), and quasilocalized vibrational modes (*43*, *44*)] and thus vary across different sites.

Unlike electromagnetic noise, phonons, as quasiparticles, follow Bose-Einstein statistics $\left[n_\omega(T) = \frac{1}{\exp(\hbar\omega/k_B T)-1}\right]$ for their number distribution. This specific characteristic enables temperature-varying experiments a powerful tool for identifying the spin-lattice relaxation over the past few decades (*44*–*46*). In particular, within the experimental temperature range (Fig. 5C), a two-phonon Raman process dominates (*43*, *44*), where the spin absorbs and subsequently emits a phonon. In this process, the generated noise fluctuations carry frequencies corresponding to the phonon energy differences, perturbing NV's spin energy. This leads to a specific temperature-dependent spin-lattice relaxation rate (S_P; Fig. 5C) characterized by the relationship $An_\omega(T)\left[n_\omega(T)+1\right]$, where A is the coupling strength (*44*).

Here, we also observe a similar temperature-dependent scaling of the emerging decoherence noise intensity ($S_E - S_P$; Fig. 5C), suggesting a distinct two-phonon Raman process–induced decoherence mechanism. However, this mechanism is primarily influenced by delocalized vibrational modes, marking a notable departure from conventional spin-lattice relaxation.

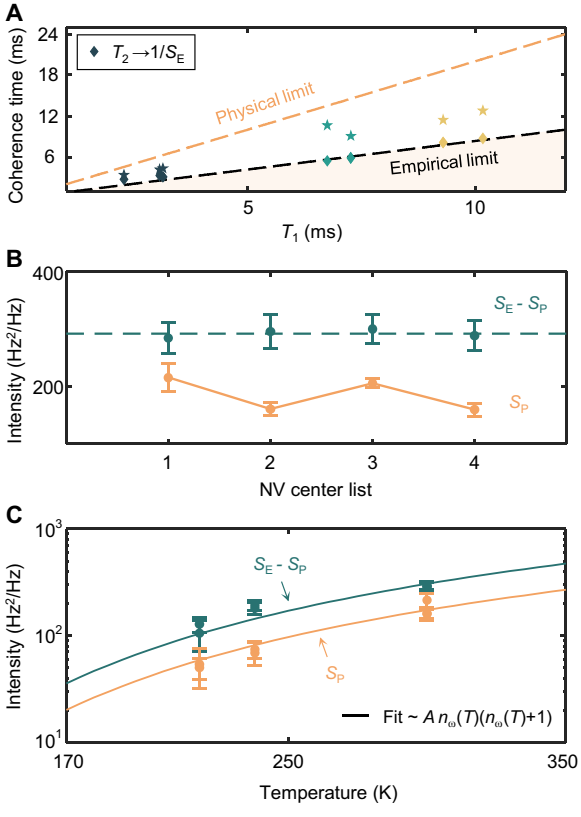

Fig. 5. A spin-lattice interaction induced decoherence. (**A**) Approaching the physical limit for various NVs at different temperatures. The dark, green, and yellow solid points represent the measured temperature of 300, 240, and 220 K, respectively. The pentagram points represent the longest $T_{2,\mathrm{CPMG}}$ achievable for each NV at the corresponding temperature. (**B**) Site dependence of noise intensity $S_E - S_P$ and S_P (fig. S6). The dashed line represents the average value of $S_E - S_P$ across different sites. (**C**) Temperature dependence of noise intensity $S_E - S_P$ and S_P (fig. S7). The distinct points at each temperature represent different NVs. Here, $n_\omega(T) = \frac{1}{\exp[\hbar\omega/k_B T]-1}$ symbolizes the Bose-Einstein distribution of phonons, with the dominant phonon energy of $\omega \approx 70$ meV within this temperature range (*44*). Also, A is the fitting spin-lattice coupling strength. All error bars are 1σ.

DISCUSSION

Discovering and characterizing the underlying mechanisms are becoming increasingly important with the advancement of solid-sate quantum technologies. Our approach provides an avenue for unraveling this intricate mechanism of diverse materials, and the observed delocalized vibrational modes in the spin-lattice interaction potentially point to size effect within the lattice. Future work will focus on further understanding and engineering this mechanism, such as the material project based on phonon modes engineering, to cultivate robust solid-state quantum devices with enhanced functionalities and performance, thus advancing the widespread applications of quantum technology. Otherwise, the results, including the developed characterization method and revealed physical mechanisms, also serve as a reference for other solid-state systems.

MATERIALS AND METHODS

Sample and experimental setup

The sample in this work is an isotopically controlled single-crystal diamond grown using chemical vapor deposition, enriched with ^{12}C to a purity of 99.999%. In this sample, the typical dephasing time is $T_2^* \approx 0.3$ ms, and the linewidth of the filter function in relaxation spectroscopy is ~5 kHz.

Magnetic resonance experiments on single NV defect spin were conducted on a homebuilt room room-temperature and low-temperature confocal setup, initialized by a 532-nm laser source (Changchun New Industries Optoelectronics Technology). The sample is positioned by an XYZ piezo-stage (C3S-D00600, nanofaktur) at low temperature and by a scanner (Physik Instrumente) at room temperature. Microwave pulses are generated by an arbitrary waveform generator (Keysight M8190A) and are fed to a gold strip line fabricated on top of the sample after amplification (minicircuit).

The empirical limit for spin $S = 1/2$ and $S = 1$ systems

The listed relaxation time in Fig. 1A represents the single-state's relaxation time, which refers to $T_1^{m_s=+1/2}$ or $T_1^{m_s=-1/2}$ for $S = 1/2$ spin systems and $T_1^{m_s=0}$ for $S = 1$ spin systems.

The coherence time $T_{2,\mathrm{CPMG}}$ discussed here is obtained through the CPMG between $m_s = 0$ and $m_s = -1$. Therefore, the relaxation time related to this $T_{2,\mathrm{CPMG}}$ should not only consider $T_1^{m_s=0}$ but also T_1 for both states (*21*, *29*). There is a distinction between $T_1^{m_s=0} = 1/\left(3\Omega_\perp\right)$ and

$T_1 = 1/(3\Omega_\perp + \gamma_\perp)$ for NV centers in diamond, which complicates the direct comparison between the empirical limit ($T_2 \approx 1/2\,T_1^{m_s=0}$) and physical limit ($T_2 = 2\,T_1$). In this case, the observation based on $\gamma_\perp/\Omega_\perp \approx 2$ (see fig. S1) provides the opportunity to build a connection of $T_1^{m_s=0} \approx (5/3)\,T_1$ in this three-level spin system. Naturally, we could reformulate the empirical limit for NV centers in diamond as $T_2 \approx (5/6)\,T_1$, as shown in Fig. 1E (black dashed line).

For a two-level spin system, it becomes straightforward as $T_1^{m_s=+1/2}$, $T_1^{m_s=-1/2}$, and T_1 are all equal, and the empirical limit remains $T_2 \approx 1/2\,T_1$.

Characterizing the site independence and temperature dependence

The complete noise spectrum in Fig. 4C includes three distinct decoherence mechanisms: impurity spin noise, spin-lattice relaxation, and emerging noise. The first two types of noise are both local, and the intensity varies randomly across different lattice sites. Because these have been extensively studied, we will not delve into it here.

For the last type, the key evidence to determine the universality of surpassing the empirical limit in Fig. 5A lies in assessing whether these noise spectra exhibit the same distribution form (cutoff frequency) across lattice points. The observations in fig. S6 demonstrate that this noise has the same distribution across different sites and exhibits identical intensity. This nonlocal nature illustrates an unprecedented noise, ensuring the universality of approaching the physical limit. Furthermore, this cutoff frequency remains consistent across varying temperatures (fig. S7B).

By extracting the intensity from the spectra across different sites at various temperatures, we obtain the site independence (Fig. 5B) and temperature dependence (Fig. 5C) of this emerging noise.

Supplementary Materials

This PDF file includes:

Sections S1 to S3
Figs. S1 to S8

REFERENCES AND NOTES

1. N. P. De Leon, K. M. Itoh, D. Kim, K. K. Mehta, T. E. Northup, H. Paik, B. S. Palmer, N. Samarth, S. Sangtawesin, D. W. Steuerman, Materials challenges and opportunities for quantum computing hardware. *Science* **372**, eabb2823 (2021).
2. A. W. Harrow, A. Montanaro, Quantum computational supremacy. *Nature* **549**, 203–209 (2017).
3. J. L. O'Brien, Optical quantum computing. *Science* **318**, 1567–1570 (2007).
4. C. L. Degen, F. Reinhard, P. Cappellaro, Quantum sensing. *Rev. Mod. Phys.* **89**, 035002 (2017).
5. J. F. Barry, J. M. Schloss, E. Bauch, M. J. Turner, C. A. Hart, L. M. Pham, R. L. Walsworth, Sensitivity optimization for NV-diamond magnetometry. *Rev. Mod. Phys.* **92**, 015004 (2020).
6. H. J. Kimble, The quantum internet. *Nature* **453**, 1023–1030 (2008).
7. S. Wehner, D. Elkouss, R. Hanson, Quantum internet: A vision for the road ahead. *Science* **362**, eaam9288 (2018).
8. D. D. Awschalom, R. Hanson, J. Wrachtrup, B. B. Zhou, Quantum technologies with optically interfaced solid-state spins. *Nat. Photonics* **12**, 516–527 (2018).
9. H. J. Mamin, M. Kim, M. H. Sherwood, C. T. Rettner, K. Ohno, D. D. Awschalom, D. Rugar, Nanoscale nuclear magnetic resonance with a nitrogen-vacancy spin sensor. *Science* **339**, 557–560 (2013).
10. J. Du, F. Shi, X. Kong, F. Jelezko, J. Wrachtrup, Single-molecule scale magnetic resonance spectroscopy using quantum diamond sensors. *Rev. Mod. Phys.* **96**, 025001 (2024).
11. W. Ji, Z. Liu, Y. Guo, Z. Hu, J. Zhou, S. Dai, Y. Chen, P. Yu, M. Wang, K. Xia, F. Shi, Y. Wang, J. Du, Correlated sensing with a solid-state quantum multisensor system for atomic-scale structural analysis. *Nat. Photonics* **18**, 230–235 (2024).
12. Y. Guo, W. Ji, X. Kong, M. Wang, H. Sun, J. Zhou, Z. Chai, X. Rong, F. Shi, Y. Wang, J. Du, Single-shot readout of a solid-state electron spin qutrit. *Phys. Rev. Lett.* **132**, 060601 (2024).
13. F. Shi, Q. Zhang, P. Wang, H. Sun, J. Wang, X. Rong, M. Chen, C. Ju, F. Reinhard, H. Chen, J. Wrachtrup, J. Wang, J. Du, Single-protein spin resonance spectroscopy under ambient conditions. *Science* **347**, 1135–1138 (2015).
14. S. Schmitt, T. Gefen, . M. Stürner, T. Unden, G. Wolff, C. Müller, J. Scheuer, B. Naydenov, M. Markham, S. Pezzagna, J. Meijer, I. Schwarz, M. Plenio, A. Retzker, L. P. McGuinness, F. Jelezko, Submillihertz magnetic spectroscopy performed with a nanoscale quantum sensor. *Science* **356**, 832–837 (2017).
15. N. Aslam, M. Pfender, P. Neumann, R. Reuter, A. Zappe, F. Fávaro De Oliveira, A. Denisenko, H. Sumiya, S. Onoda, J. Isoya, J. Wrachtrup, Nanoscale nuclear magnetic resonance with chemical resolution. *Science* **357**, 67–71 (2017).
16. C. E. Bradley, J. Randall, M. H. Abobeih, R. C. Berrevoets, M. J. Degen, M. A. Bakker, M. Markham, D. J. Twitchen, T. H. Taminiau, A ten-qubit solid-state spin register with quantum memory up to one minute. *Phys. Rev. X* **9**, 031045 (2019).
17. D. R. Glenn, D. B. Bucher, J. Lee, M. D. Lukin, H. Park, R. L. Walsworth, High-resolution magnetic resonance spectroscopy using a solid-state spin sensor. *Nature* **555**, 351–354 (2018).
18. S. Kolkowitz, A. Safira, A. A. High, R. C. Devlin, S. Choi, Q. P. Unterreithmeier, D. Patterson, A. S. Zibrov, V. E. Manucharyan, H. Park, M. D. Lukin, Probing johnson noise and ballistic transport in normal metals with a single-spin qubit. *Science* **347**, 1129–1132 (2015).
19. J. Rovny, Z. Yuan, M. Fitzpatrick, A. I. Abdalla, L. Futamura, C. Fox, M. C. Cambria, S. Kolkowitz, N. P. de Leon, Nanoscale covariance magnetometry with diamond quantum sensors. *Science* **378**, 1301–1305 (2022).
20. G. Balasubramanian, P. Neumann, D. Twitchen, M. Markham, R. Kolesov, N. Mizuochi, J. Isoya, J. Achard, J. Beck, J. Tissler, V. Jacques, P. R. Hemmer, F. Jelezko, J. Wrachtrup, Ultralong spin coherence time in isotopically engineered diamond. *Nat. Mater.* **8**, 383–387 (2009).
21. E. D. Herbschleb, H. Kato, Y. Maruyama, T. Danjo, T. Makino, S. Yamasaki, I. Ohki, K. Hayashi, H. Morishita, M. Fujiwara, N. Mizuochi, Ultra-long coherence times amongst room-temperature solid-state spins. *Nat. Commun.* **10**, 3766 (2019).
22. L. Viola, E. Knill, S. Lloyd, Dynamical decoupling of open quantum systems. *Phys. Rev. Lett.* **82**, 2417–2421 (1999).
23. L. Viola, S. Lloyd, Dynamical suppression of decoherence in two-state quantum systems. *Phys. rev. A* **58**, 2733–2744 (1998).
24. J. Du, X. Rong, N. Zhao, Y. Wang, J. Yang, R. B. Liu, Preserving electron spin coherence in solids by optimal dynamical decoupling. *Nature* **461**, 1265–1268 (2009).
25. C. P. Anderson, E. O. Glen, C. Zeledon, A. Bourassa, Y. Jin, Y. Zhu, C. Vorwerk, A. L. Crook, H. Abe, J. Ul-Hassan, T. Ohshima, N. T. Son, G. Galli, D. D. Awschalom, Five-second coherence of a single spin with single-shot readout in silicon carbide. *Sci. Adv.* **8**, eabm5912 (2022).
26. A. M. Tyryshkin, S. Tojo, J. J. L. Morton, H. Riemann, N. V. Abrosimov, P. Becker, H. J. Pohl, T. Schenkel, M. L. W. Thewalt, K. M. Itoh, S. A. Lyon, Electron spin coherence exceeding seconds in high-purity silicon. *Nat. Mater.* **11**, 143–147 (2012).
27. A. Gottscholl, M. Diez, V. Soltamov, C. Kasper, A. Sperlich, M. Kianinia, C. Bradac, I. Aharonovich, V. Dyakonov, Room temperature coherent control of spin defects in hexagonal boron nitride. *Sci. Adv.* **7**, eabf3630 (2021).
28. P. Siyushev, K. Xia, R. Reuter, M. Jamali, N. Zhao, N. Yang, C. Duan, N. Kukharchyk, A. D. Wieck, R. Kolesov, J. Wrachtrup, Coherent properties of single rare-earth spin qubits. *Nat. Commun.* **5**, 3895 (2014).
29. N. Bar-Gill, L. M. Pham, A. Jarmola, D. Budker, R. L. Walsworth, Solid-state electronic spin coherence time approaching one second. *Nat. Commun.* **4**, 1743 (2013).
30. D. D. Sukachev, A. Sipahigil, C. T. Nguyen, M. K. Bhaskar, R. E. Evans, F. Jelezko, M. D. Lukin, Silicon-vacancy spin qubit in diamond: A quantum memory exceeding 10 ms with single-shot state readout. *Phys. Rev. Lett.* **119**, 223602 (2017).
31. J. R. Klauder, P. W. Anderson, Spectral diffusion decay in spin resonance experiments. *Phys. Rev.* **125**, 912–932 (1962).
32. G. A. Álvarez, D. Suter, Measuring the spectrum of colored noise by dynamical decoupling. *Phys. Rev. Lett.* **107**, 230501 (2011).
33. J. Bylander, S. Gustavsson, F. Yan, F. Yoshihara, K. Harrabi, G. Fitch, D. G. Cory, Y. Nakamura, J. S. Tsai, W. D. Oliver, Noise spectroscopy through dynamical decoupling with a superconducting flux qubit. *Nat. Phys.* **7**, 565–570 (2011).
34. T. Xie, Z. Zhao, M. Guo, M. Wang, F. Shi, J. Du, Identity test of single NV^- centers in diamond at Hz-precision level. *Phys. Rev. Lett.* **127**, 053601 (2021).
35. B. A. Myers, A. Ariyaratne, A. C. B. Jayich, Double-quantum spin-relaxation limits to coherence of near-surface nitrogen-vacancy centers. *Phys. Rev. Lett.* **118**, 197201 (2017).
36. L. T. Hall, P. Kehayias, D. A. Simpson, A. Jarmola, A. Stacey, D. Budker, L. C. L. Hollenberg, Detection of nanoscale electron spin resonance spectra demonstrated using nitrogen-vacancy centre probes in diamond. *Nat. Commun.* **7**, 10211 (2016).
37. G. De Lange, Z. H. Wang, D. Ristè, V. V. Dobrovitski, R. Hanson, Universal dynamical decoupling of a single solid-state spin from a spin bath. *Science* **330**, 60–63 (2010).

38. M. Kim, H. J. Mamin, M. H. Sherwood, K. Ohno, D. D. Awschalom, D. Rugar, Decoherence of near-surface nitrogen-vacancy centers due to electric field noise. *Phys. Rev. Lett.* **115**, 087602 (2015).
39. N. Zhao, S. W. Ho, R. B. Liu, Decoherence and dynamical decoupling control of nitrogen vacancy center electron spins in nuclear spin baths. *Phys. Rev. B* **85**, 115303 (2012).
40. E. Bauch, S. Singh, J. Lee, C. A. Hart, J. M. Schloss, M. J. Turner, J. F. Barry, L. M. Pham, N. Bar-Gill, S. F. Yelin, R. L. Walsworth, Decoherence of ensembles of nitrogen-vacancy centers in diamond. *Phys. Rev. B* **102**, 134210 (2020).
41. R. Li, F. Kong, P. Zhao, Z. Cheng, Z. Qin, M. Wang, Q. Zhang, P. Wang, Y. Wang, F. Shi, J. Du, Nanoscale electrometry based on a magnetic-field-resistant spin sensor. *Phys. Rev. Lett.* **124**, 247701 (2020).
42. P. Jamonneau, M. Lesik, J. P. Tetienne, I. Alvizu, L. Mayer, A. Dréau, S. Kosen, J.-F. Roch, S. Pezzagna, J. Meijer, T. Teraji, Y. Kubo, P. Bertet, J. R. Maze, V. Jacques, Competition between electric field and magnetic field noise in the decoherence of a single spin in diamond. *Phys. Rev. B* **93**, 024305 (2016).
43. J. Zhang, C. Z. Wang, Z. Z. Zhu, V. V. Dobrovitski, Vibrational modes and lattice distortion of a nitrogen-vacancy center in diamond from first-principles calculations. *Phys. Rev. B* **84**, 035211 (2011).
44. M. C. Cambria, A. Norambuena, H. T. Dinani, G. Thiering, A. Gardill, I. Kemeny, Y. Li, V. Lordi, Á. Gali, J. R. Maze, S. Kolkowitz, Temperature-dependent spin-lattice relaxation of the nitrogen-vacancy spin triplet in diamond. *Phys. Rev. Lett.* **130**, 256903 (2023).
45. M. B. Walker, A T^5 spin–lattice relaxation rate for non-Kramers ions. *Can. J. Phys.* **46**, 1347–1353 (1968).
46. A. Norambuena, E. Muñoz, H. T. Dinani, A. Jarmola, P. Maletinsky, D. Budker, J. R. Maze, Spin-lattice relaxation of individual solid-state spins. *Phys. Rev. B* **97**, 094304 (2018).

Acknowledgments

Funding: This work was supported by the National Natural Science Foundation of China (grants nos. T2325023, 92265204, T2388102, 12104446, 12104447, and 12261160569), the Innovation Program for Quantum Science and Technology (grant no. 2021ZD0302200), the Fundamental Research Funds for the Central Universities, the China Postdoctoral Science Foundation (grant no. 2024M753084), and the Postdoctoral Fellowship Program of CPSF (grant no. GZB20240717). **Author contributions:** J.D. and Y.W. supervised the project. Y.W. conceived the idea. Y.W. and S.H. designed the experiment. S.H., W.J., Y.G., and Z.L. prepared the setup. S.H. performed the experiments and analyzed the data. X.Y. and M.W. prepared the sample. Y.W., S.H., X.Z., and J.D. wrote the manuscript. All authors discussed the results and commented on the manuscript. **Competing interests:** The authors declare that they have no competing interests. **Data and materials availability:** All data needed to evaluate the conclusions in the paper are present in the paper and/or the Supplementary Materials.

Submitted 22 July 2024
Accepted 28 January 2025
Published 28 February 2025
10.1126/sciadv.adr9298